GEOLOGIC NOTES

Composition of seismic facies: A case study

Ståle Emil Johansen

ABSTRACT

In this case study, we used simulated seismic data from outcrops on Svalbard to analyze what seismic facies are composed of, what the dominating factors in forming the facies are, and which consequences this has for the interpretation results. Seismic facies analyses can be used to interpret environmental setting, depositional processes, and lithology. Here, we found that noise is the most important factor in forming the seismic facies. Noise is defined as all reflections that cannot be ascribed directly to the reservoir model. Effects from overburden and processing dominated, and the low-frequency content of the seismic section complicated the seismic facies analyses. The main reason for this is that the analysis relies heavily on identified internal patterns and low-angle terminations. Such patterns and terminations are easily created by the seismic method itself, by overburden effects, and by artifacts generated when processing the data. External form, strong amplitudes, and continuous reflections are robust seismic observations, whereas the internal pattern and terminations are commonly deceptive. Identification of boundaries based on predefined patterns of terminations does not work here, and uncritical use of seismic facies analysis in this interpretation case will create wrong reservoir models. Because of the size of the outcrops, the results from this analysis are relevant for reservoir-scale seismic interpretation and detailed interpretation for prospect evaluation in mature basins. For seismic interpretation at a more regional scale, it is probably less relevant.

Manuscript received July 16, 2012; provisional acceptance October 5, 2012; revised manuscript received January 9, 2013; final acceptance March 27, 2013.
DOI:10.1306/03271312119

AUTHOR

Ståle Emil Johansen ~ *Norwegian University of Science and Technology, Department of Petroleum Engineering and Applied Geophysics, Trondheim, Norway; stale.johansen@ntnu.no*

Ståle Emil Johansen is a professor in applied geophysics at the Institute of Petroleum Engineering and Applied Geophysics, Norwegian University of Science and Technology. His current research is focused on geophysical expressions of subsurface terrains and the development of sedimentary basins in the Arctic region. Before joining the university, he worked for Statoil and Electromagnetic Geoservices (EMGS).

ACKNOWLEDGEMENTS

I thank Stig Arne Karlsen and Anwar Hossain Bhuiyan for valuable help in preparing the figures for this manuscript.
The AAPG Editor thanks the following reviewers for their work on this paper: Stephen P. Cumella and an anonymous reviewer.

INTRODUCTION

Seismic facies are mappable three-dimensional seismic units composed of groups of reflections whose parameters differ from those of adjacent facies units. Where the internal reflection parameters, the external form, and the three-dimensional associations of these seismic units are delineated, the units can be interpreted in terms of environmental setting, depositional processes, and estimates of lithology (Mitchum et al., 1977). In its original form, seismic facies analysis should be performed within the framework of depositional sequence analysis. Over the years, the technique has developed into a more general technique for describing, organizing, and interpreting seismic observations.

Stratigraphic conclusions from seismic data depend on the data being sufficiently free of noise so that the seismic response is predominantly that of the sediments. Thus, good recording and processing is essential (Sheriff, 1977). Forward seismic modeling allows testing of the relationship between geology and seismic response and is potentially very well suited for testing of interpretation methodology. To get the best possible synthetic data, simulations were based on a geologic model from well-exposed and well-documented outcrops from Van Keulenfjorden, Svalbard, in the Norwegian Arctic.

Here, we analyze and discuss what the seismic facies in the synthetic seismic section are composed of and what the dominating factors in forming the facies are. We discuss the influence of noise and compare it to the influence of primary reflections from lithologic boundaries. Noise is here defined as all reflections that cannot be ascribed directly to the reservoir model. In our discussion of noise, we focus on the effects that frequency content, overburden, and data processing have on the interpretation result.

MODELING OF OUTCROPS

Forward modeling on models from well-exposed and well-documented outcrops was first presented by Biddle et al., 1992 and Johansen et al., 1994.

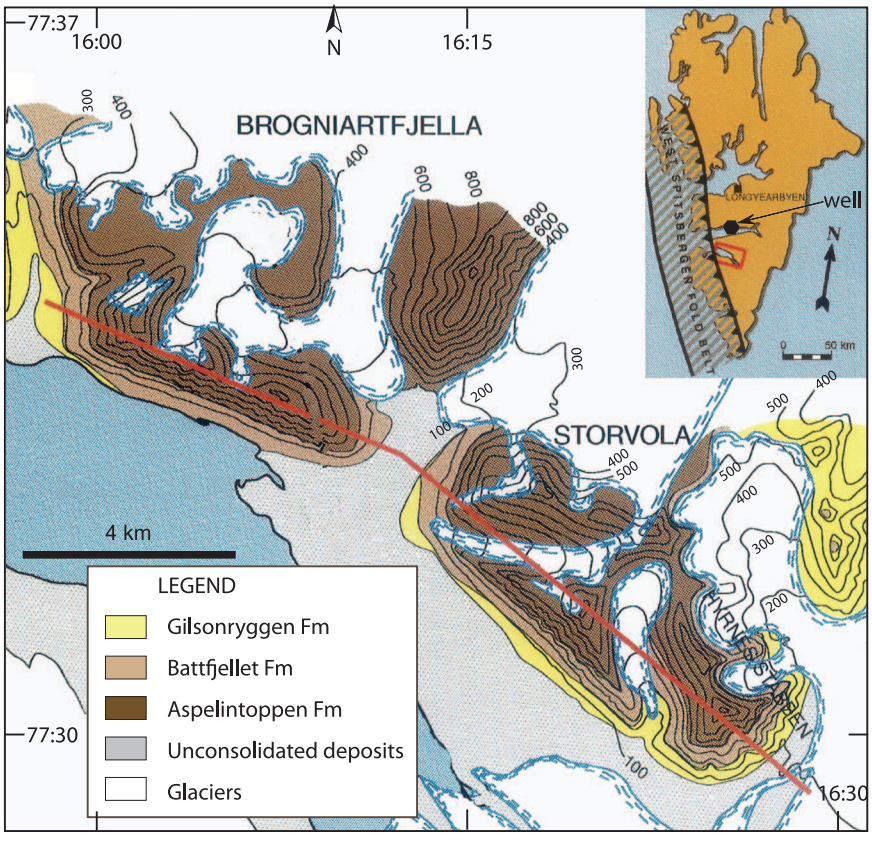

Figure 1. Locality map of Van Keulenfjorden exposures on Spitsbergen, Svalbard. The Brogniartfjellet, Storvola, and Hyrnestabben outcrops consist of clinoforms reflecting Eocene infilling of the Central Basin. Note the well symbol north of the red rectangle marking the study area. Contours in meters above sea level. Fm = Formation.

The steps in a fully integrated outcrop study consist of (1) geologic fieldwork, (2) photogrammetry, (3) petrophysical analysis, (4) seismic modeling, (5) seismic processing, and (6) seismic interpretation (Johansen et al., 2007). Van Keulenfjorden, Spitsbergen, at the northwestern corner of the Barents Sea platform, is an excellent location for such studies (Figure 1). For a general overview of the geology of the Barents Sea region, see Johansen et al., 1993.

Outcrops

The latest Paleocene–early Eocene infilling of the Central Basin on Spitsbergen progressed from west to east and left a spectacular record of large-scale shallow- to deep-water clinoforms. These are now exposed along the northern mountain side of the fjord (Figure 2). For details on the Tertiary development of Svalbard, see also Kellog, 1975; Myhre et al., 1982; Spencer et al., 1984; and Steel et al., 1985.

Mountainside architecture appears rather simple when seen from a distance. A lower poorly exposed marine shale unit is overlain by shoreface sandstones, again overlain by thin fluvial sandstone lenses in a matrix of floodplain fines. However, the photogrammetry (Dueholm, 1990, 1992; Dueholm and Olsen, 1993) step of the integrated outcrop study revealed a significant complexity in the exposed rocks. Sedimentologic sections were also measured, and key lithologies, facies associations, and a sequence-stratigraphic framework were established (Figure 3). Further details of the outcrops are discussed in Steel et al. (2000), Steel and Olsen (2002), and Mellere et al. (2003).

Impedance Model

Velocity and density variations from the outcrops were constrained by laboratory measurements of rock samples and velocity logs from one well (Figure 1). P-wave (compressional wave) velocity, S-wave (shear wave) velocity, and densities were measured on representative lithologies. The results of the velocities and density measurements are shown in Table 1. Vertical impedance contrasts are

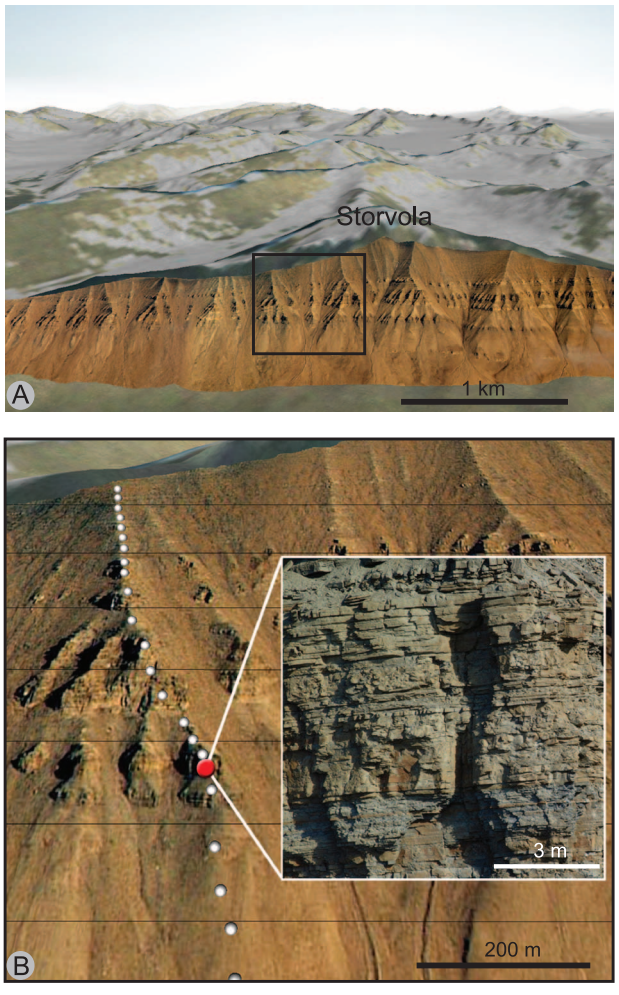

Figure 2. Photograph mosaic of Tertiary exposures in Van Keulenfjorden. The top of the Storvola Mountain can be used as reference when comparing with Figure 3.

well controlled, but lateral variations are difficult to sample correctly in the field and are therefore less well constrained. The structure and mountain topography were removed, and the resulting "reservoir model" is shown in Figure 4. A second model (buried model) was made by burying the reservoir model under 1100 to 1400 m (3609–4593 ft) of overburden rocks. This was performed using P-wave velocities, S-wave velocities, and densities from Tertiary strata drilled by a North Sea well. All layers in the overburden are continuous, and a water layer was added on top of the model (Figure 5).

Estimation of velocity and density distribution is difficult. These parameters vary in three dimensions, and values assigned to a given layer must be

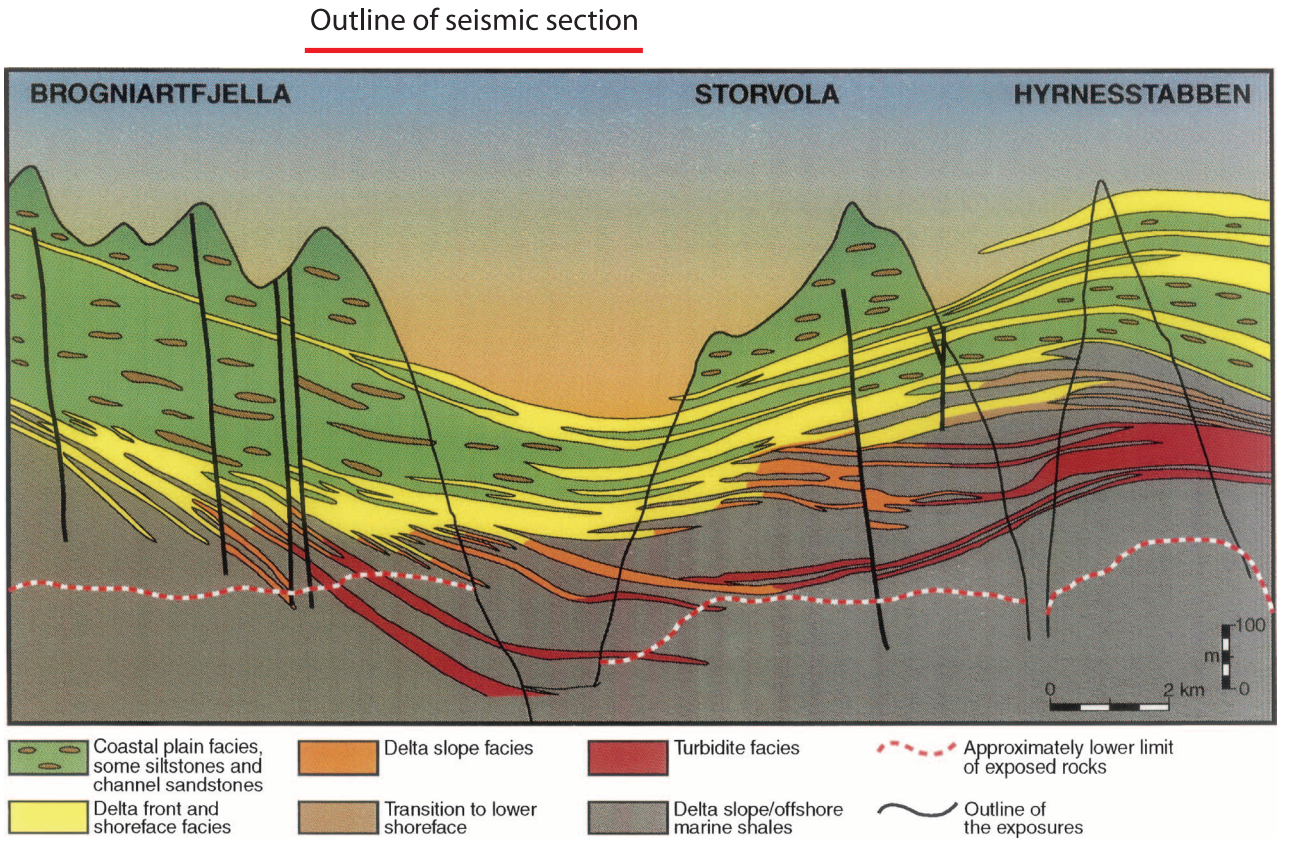

Figure 3. Facies model of Van Keulenfjorden outcrops. The corresponding rock properties are given in Table 1. See Figure 1 for the location of profile.

considered an approximation. Implicit in this process is the assumption that acoustic impedance is directly related to lithology. Other factors such as pore-fluid composition and pore pressure also have effects on the acoustic impedance, but such factors are not fully considered in this study. However, the values used are representative for the individual facies, and the resulting impedance contrasts are comparable to contrasts seen in well logs from similar geologic settings. For more details, see Johansen et al. (2007).

Seismic Simulation

Two types of modeled data sets were used in this study. (1) The reflectivity section derived from the impedance model (reservoir model) was convolved with a minimum-phase Ricker wavelet. The resulting seismic section assumes vertical incidence to surfaces (image ray modeling) and simulates a migrated seismic section. (2) A high-frequency (100 Hz) and a low-frequency (30 Hz) section were generated (Figures 6, 7). The other seismic models were generated by a two-dimensional (2-D) elastic wave propagation modeler that uses a high-order space and a second-order time finite-difference scheme (Mittet and Renlie, 1996).

The inputs to the 2-D modeler are grids of P-wave velocity, S-wave velocity, and density from the buried model. The grid size is 2 × 2 m (7 × 7 ft). The average frequency content in the target area is approximately 30 Hz. A standard 2-D marine acquisition was simulated with recording parameters given in Table 2. To imitate industry workflow, the processing was performed by industry providers outside the project (Table 3). Vien et al. (1997) discuss the aspects of the processing of this data set in detail, but their processing sequence was different from the ones used in this study. For more details on the limitations and sources of error in forward modeling, see Cerjan et al. (1985), Holberg (1987), and Mittet and Renlie (1996).

Table 1. P-Wave Velocities, S-Wave Velocities, and Densities Selected for Input to the Seismic Modeling

Lithology/Facies Association	P-Wave Velocity	S-Wave Velocity	Density	V_p/V_s	Basis for Choosing Values
Turbidite facies	3.69	2.53	2.6	1.458	Average values within this type of facies (from petrophysical measurements)
Delta-slope facies	3.42	2.26	2.6	1.513	Average values within this type of facies (from petrophysical measurements)
Fluvial sandstones (within the coastal plain Aspelin-Toppen Formation)	3.33	2.51	2.6	1.327	Average values within this type of facies (from petrophysical measurements)
Shoreface/delta-front facies	3.29	2.31	2.6	1.424	Average values within this type of facies (from petrophysical measurements)
Lower shoreface hetereoliths (transition to lower shoreface)	3.07	2.21	2.6	1.389	Average values within this type of facies (from petrophysical measurements)
Delta-front/offshore marine shales	2.77	1.9	2.5	1.458	P-wave and S-wave velocities are 75% of the value used for the turbidite sandstones. This is in relationship with what is seen in the Ishøgda well.
Coastal plain shales and siltstones (Aspelin-Toppen Formation)	2.47	1.73	2.5	1.428	P-wave and S-wave velocities are 75% of the value used for the turbidite sandstones. This is in relationship with what is seen in the Ishøgda well.
Seawater	1.5	0	1		

SEISMIC FACIES, INTERPRETATION, AND DISCUSSION

In its original form, seismic facies analysis should be performed within the framework of depositional sequence analysis. Over the years, the technique has developed into a more general technique for describing, organizing, and interpreting seismic observations. In the following sections, we analyze and discuss in detail what the seismic facies in the synthetic seismic section are composed of and what the dominating factors in forming the facies are.

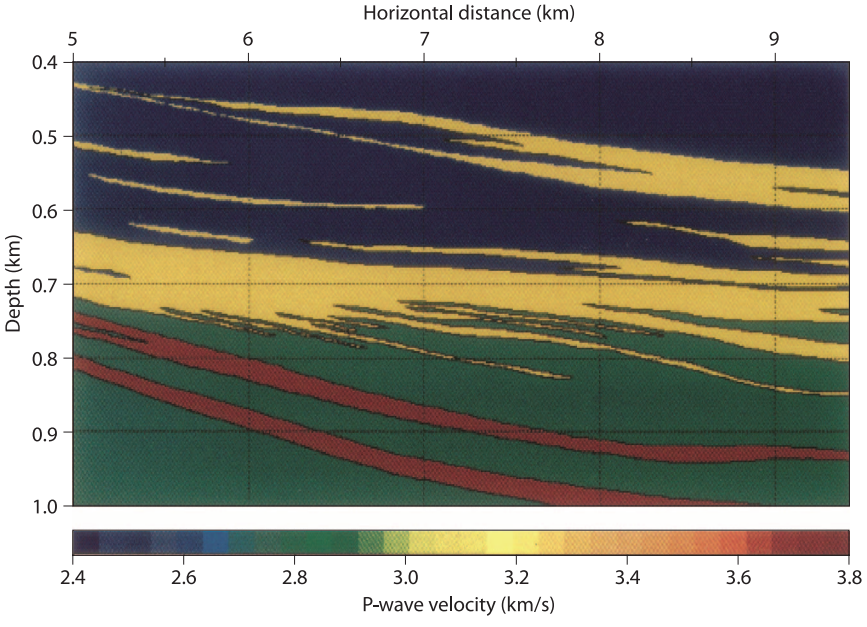

Figure 4. P-wave (compressional or primary wave) velocity model of Van Keulenfjorden outcrops (reservoir model). See Figure 3 for comparison with stratigraphic and lithologic models and Figure 1 for the location of the profile. Because the density variations are minor, this section also illustrates impedance variations very well.

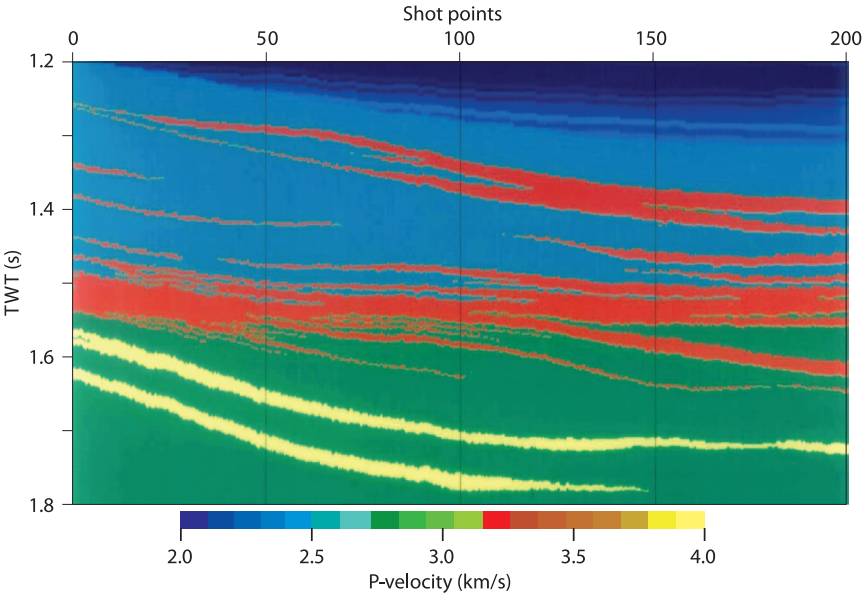

Figure 5. P-wave velocity model of Van Keulenfjorden outcrops (reservoir model) combined with a constructed overburden (overburden model). Velocity distribution in the overburden is representative for Tertiary strata in the northern North Sea. See Figure 3 for comparison with stratigraphic and lithologic models, and Figure 1 for location of profile. Because the density variations are minor, this section also illustrates the impedance variations very well. See Johansen et al. (2007) for more details on the overburden model. TWT = two-way traveltime.

Primary Reflections

Figure 6 shows the high-frequency response to the lithologic succession shown in Figure 4 (reservoir model). The corresponding depositional facies are shown in Figure 3. The top and base of thin sandstone units create constructive interference, but beyond that, the 100-Hz image gives a clear and exact seismic representation of the depositional model.

The deep-marine turbidite sandstones are represented by two continuous reflections (A, A′). The delta-front and shoreface facies pinching out into delta-slope and offshore marine shales show a clear prograding pattern (BB′), with eastward thinning and downlap onto reflection A. The downlap pattern is most evident on the low-frequency seismic section (Figure 7, eastern part).

The coastal-plain sandstones (C, C′, C″) occur as scattered and discontinuous reflections in a neutral background of reflection-free coastal-plain facies (D). In the upper part of the section, a transgression causes more delta-front and shoreface facies to be

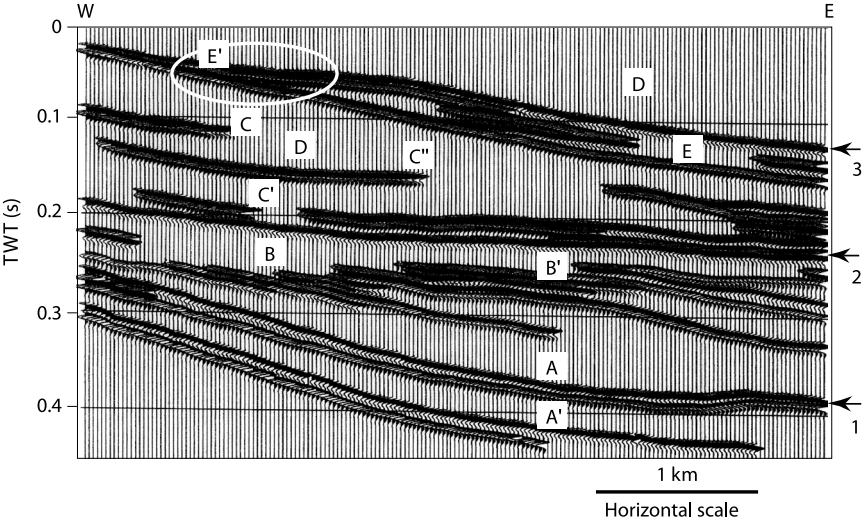

Figure 6. Synthetic seismic section (100 Hz) of the velocity model in Figure 4. The reflectivity section derived from the impedance model was convolved by a minimum-phase Ricker wavelet. Because the resulting seismic section assumes vertical incidence to surfaces (image-ray modeling), the section simulates a migrated seismic line. In Figures 6–10, for easier reference, three reflectors are marked by horizontal black arrows and marked 1, 2, and 3. See text for the explanation of reflection numbering and letters. Arrows, ellipses, and circles in Figures 6–10 represent important observations and are also explained in the text. TWT = two-way traveltime.

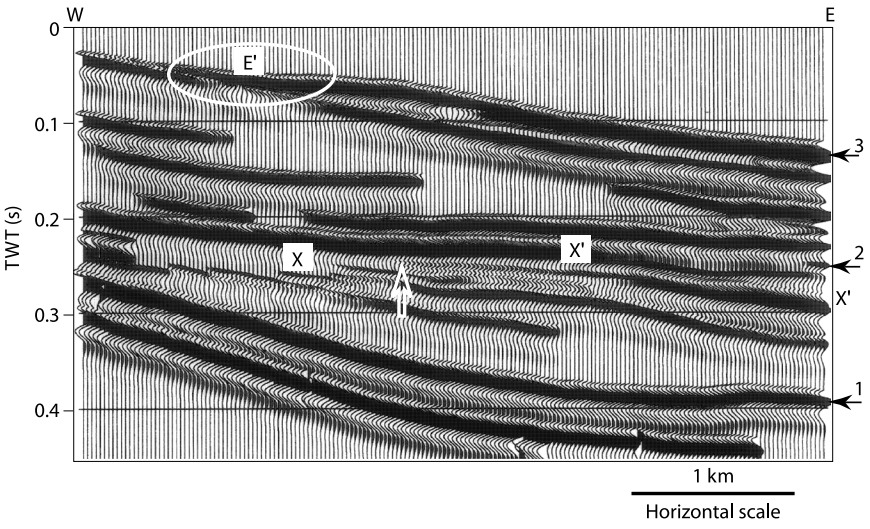

Figure 7. Synthetic seismic section (30 Hz) of the velocity model in Figure 4. The reflectivity section derived from the impedance model was convolved by a minimum-phase Ricker wavelet. Because the resulting seismic section assumes vertical incidence to surfaces (image-ray modeling), the section simulates a migrated seismic line. In Figures 6–10, for easier reference, three reflectors are marked by horizontal black arrows and marked 1, 2, and 3. See also the text for the explanation of numbering and letters. Arrows, ellipses, and circles in Figures 6–10 represent important observations and are also explained in the text. TWT = two-way traveltime.

deposited. This event is clearly imaged as a thinning and onlapping seismic event (EE′).

Noise, multiples, and conversions are not included in this simulation, and in the real world, one cannot expect to get as high a frequency and as exact a seismic section as shown in Figure 6. The closest one could get is shallow high frequency seismic acquired for research, geotechnical purposes, or for drilling hazard reasons. Normally, this is outside the depth range for hydrocarbon prospecting.

Burial Depth

The low-frequency image of the reservoir model (Figure 7) simulates burial to a realistic depth for a hydrocarbon reservoir. Constructive and destructive interference now occur between top and base reflections for all potential reservoir sandstones. Because of the lower and more realistic frequency content (30-Hz center frequency), this seismic appears continuous as new reflections are added. For example, the reflections between X and X′ make the prograding delta front and shoreface facies appear more continuous on the seismic section than they are in the impedance model. These new reflections also create apparent top lap and truncation (white arrow in Figure 7) not present in the geologic model (Figures 3–5). Few changes occur in the upper section other than increased continuity caused by lower resolution. The seismic expression of the transgressive sands becomes less detailed compared to the 100-Hz image, and onlap E′ (Figure 6) appears more like a truncation in the 30-Hz image (Figure 7).

Table 2. Seismic Acquisition Parameters for the Modeled Seismic Sections (Finite-Difference Modeling Algorithm)

Parameter	Amount
Source depth	10 m
Shot interval	25 m
Maximum frequency content	80 Hz
Cable depth	10 m
Near offset	0 m
Far offset	2000 m
Group interval	12.5 m
Record length	3000 ms

Overburden and Processing

The overburden sections (Figures 8, 9) are based on exactly the same reservoir model as the sections in Figures 6 and 7. In addition, realistic marine acquisition has been simulated, the data have been processed, and the seismic energy has passed through the overburden twice before being recorded. The changes are rather significant, and the new seismic sections are very different from the simpler images previously presented. However, many of the primaries (Figure 6) are fortunately present in the

Table 3. Processing Sequences for the Modeled Seismic Sections (Finite-Difference Modeling Algorithm)*

Original Version	Reprocessed Version
1. Pre-deconvolution ramp including inside trace ramp	1. Data input
2. Normal moveout correction using dip moveout correction velocities	2. Geometry merge
3. Dip moveout correction	3. True amplitude recovery
4. Deconvolution before stacking	$T^{1.0}$ gain function to 3000 ms
Prediction gap: 24 ms	4. Trace mute: near trace high-amplitude muting
Active operator length: 240 ms	5. Trace mute: direct arrival muting
5. Normal moveout correction using stacking velocities	6. Normal moveout correction
6. Stack mute	7. Trace mute: pre-demultiple muting
7. Deconvolution after stacking	8. Band pass filter: 10-Hz (18-db/octave)–60-Hz
Prediction gap: 24 ms	(72-dB/octave) minimum phase Butterworth filter
Active operator length: 240 ms	9. FK filter: FK fan filter – 750,000–0.1 m/s, 5–90 Hz
8. Inverse Q-filter	pass zone 90% flat
Q-factor: 280	10. Inverse normal moveout correction
Constant in entire time window	11. Normal moveout correction
9. Migration	12. Trace mute: stacking mute with 30-ms time ramp
Finite-difference algorithm applied in S-F domain.	13. CMP stack.
10. Display mute	14. Band pass filter: 8-Hz (18-dB/octave)–60-Hz
11. Residual gain correction: 5 dB/s	(72-dB/octave) minimum phase Butterworth filter
	15. Migration: finite-difference migration
	16. Plot

*FK = frequency-wave number; S-F = space-frequency; CMP = common midpoint.

complex seismic images. Two different processing sequences have been applied to the data (Table 3). The original version is shown in Figure 8, and the reprocessed version, in Figure 9. The original version was processed on a normal industry contract. The reprocessing was performed by another processing team, and here, the exact velocity model was given to the processors.

In the original version, the continuity in the data is poor, and it is difficult to trace reflections over some distance. For the deep-water reservoir, it is only the upper sand (reflection 1) that is clearly visible in the section. For the lower sand, the primary reflection interferes with noise, and the seismic response is distorted. The next reflection that can be traced with confidence is reflection 2. This is the top of the prograding delta front and shoreface facies. The package between the two reflections is clearly thinning toward the west, and despite the noisy and chaotic reflection pattern, a prograding trend can also be observed in this image. However, the toplap (ellipses), much of the internal pattern, and all terminations against the boundaries (e.g., onlap and arrows) are not real. Such observations are critical for the seismic facies analysis.

In the reprocessed version (Figure 9), the general pattern has changed. This section is much more continuous than the original version (Figure 8). Both the noise and the primaries are now displayed as continuous reflections. The deep-water sands (reflection 1 and below) stand out with high amplitudes. The pattern in the lower part of the space between reflections 1 and 2 appears as an infilling pattern with onlap onto the upper deep-marine sand. This pattern is not real, and the internal reflections are noise (downward arrows). In the upper part of the interval, reflection decoupling occurs (stippled circle; see also Figure 10 for reference), and the toplap terminations (arrows) are false. The apparent terminations are against the following cycle from the top surface of the prograding delta-front and shoreface facies. The upper part of this facies appears much more continuous on the seismic section than it really is.

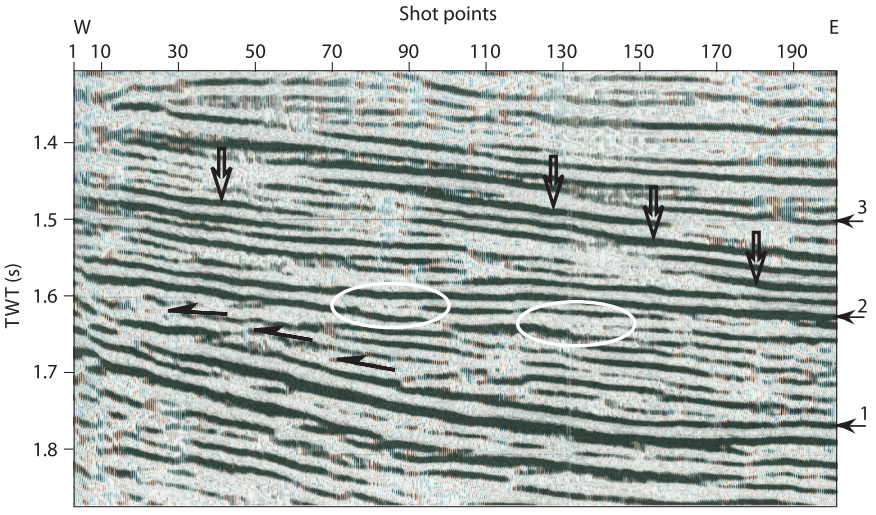

Figure 8. Synthetic seismic section (finite-difference modeling algorithm) of the model shown in Figure 5 (overburden model). In Figures 6–10, for easier reference, three reflectors are marked by horizontal black arrows and marked 1, 2, and 3. Arrows, ellipses, and circles in Figures 6–10 represent important observations and are explained in the text. TWT = two-way traveltime.

The next unit between reflections 2 and 3 is dominated by fine-grained fluvial facies with backstepping delta-front and shoreface facies on top. The top of this sand makes up the upper boundary of the unit. In the original image (Figure 8, reflection 3), it is difficult to pick this boundary, whereas it is prominent in the reprocessed version (Figure 9, reflection 3). We know from the primaries (Figures 6, 7) that large parts of the unit ideally should be reflection free with scattered reflections from fluvial channel sandstones. In the broad picture, this is, to some extent, also the case for the original seismic section. The high-amplitude reflections from the sands are marked with downward arrows in Figure 8. These amplitudes are much more smeared into continuous reflections in the reprocessed seismic section (zigzag arrows in Figure 9) and are more difficult to interpret correctly.

Surfaces and Boundaries

We see from the general depositional model in Figure 3 that the lower and middle parts of the section in Figure 4 are dominated by regression and, to some extent, by aggradation, whereas the upper part consists of an aggrading package followed by transgression. Based on field work, a sequence-stratigraphic depositional framework was established for these outcrops (e.g., Johansen et al., 2007). From the sequence-stratigraphic model, three significant surfaces were identified (numbered 1, 2, and 3 in Figures 6–10). The lower is a

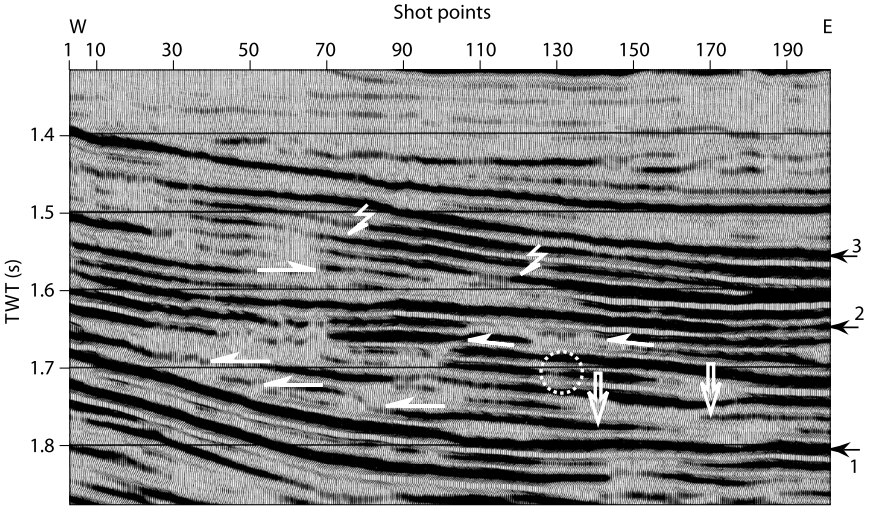

Figure 9. Synthetic seismic section (finite-difference modeling algorithm) of the model shown in Figure 5 (overburden model), reprocessed version. In Figures 6–10, for easier reference, three reflectors are marked by horizontal black arrows and marked 1, 2, and 3. Arrows, ellipses, and circles in Figures 6–10 represent important observations and are explained in the text. TWT = two-way traveltime.

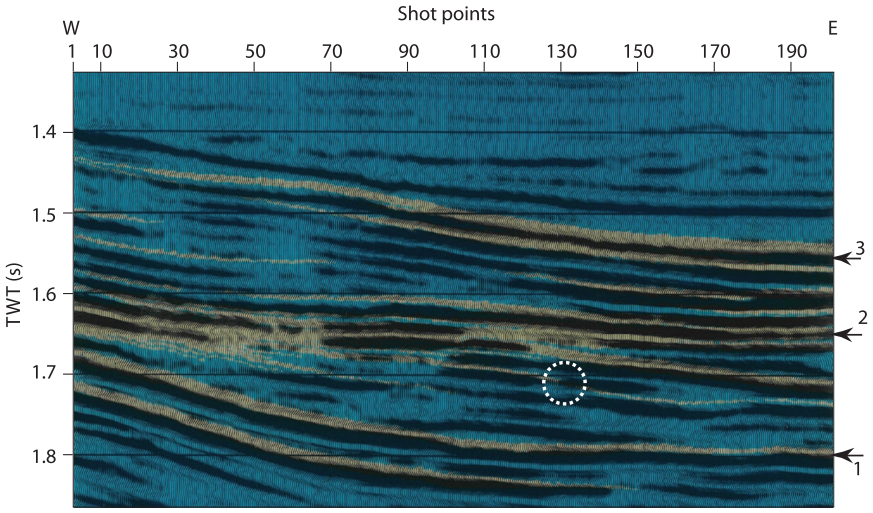

Figure 10. Synthetic seismic section (finite-difference modeling algorithm) identical with the section in Figure 9 combined with the P-wave velocity model in Figure 5. The color scale for the velocity model is compressed to distinguish sandy facies (yellow) from shales (blue). In Figures 6–10, for easier reference, three reflectors are marked by horizontal black arrows and marked 1, 2, and 3. Arrows, ellipses, and circles in Figures 6–10 represent important observations and are explained in the text. TWT = two-way traveltime.

downlap surface (DLS), the middle is a sequence boundary (SB), and the upper is a maximum flooding surface.

In the velocity models (Figures 4, 5), the DLS is not a clear DLS. The downward-dipping units stop long before they reach sandstone A (Figure 6). The reflection that stops above letter A in Figure 6 is in the low-frequency image (Figure 7), extended by the following cycle from the prograding unit above. In this way, artificial downlap is created. This is an effect commonly seen in simulated seismic data. Figure 10 shows that no direct terminations exist against the DLS that have their origins in primary reflections from the geologic model.

In the sequence-statigraphic depositional model, several high-order sequence boundaries were interpreted. The best candidate for seismic identification is a boundary represented by reflection 2 in Figures 6–10. This boundary coincides with the top of the sand-prone prograding delta-front and shoreface facies. The reflections from the prograding units and the cycle overlaying the SB create a toplap-truncation pattern (Figure 7). This pattern is, to some extent, also preserved in Figures 8 and 9, but interference with other low-angle reflections complicates the picture. Based on standard seismic facies analysis (SFA) criteria alone, it is difficult to identify the SB correctly on the seismic section, and a surface defined by the toplap will place the SB within the prograding unit.

In the seismic data, the transgressive and aggrading sections between reflections 2 and 3 are not associated with SFA terminations as such but are characterized by strong amplitudes climbing in the section in a westward direction. This pattern is robust and survives low-frequency effects (Figure 7) and both of the processing schemes (Figures 8–10).

Lessons Learned

All the simulated seismic sections are realizations of the reservoir model in Figure 4. Except for the 100-Hz image, the seismic sections are complex combinations of primaries and noise. Noise is here defined as all reflections that cannot be ascribed directly to the reservoir model. We find that noise is the dominating factor in forming the seismic facies, and much of this noise is unavoidable because it is created by the seismic method itself. The noise is also easily misinterpreted as terminations and internal patterns that have geologic meaning in an SFA context.

The step from a simple reflectivity section to a seismic section created by finite-difference modeling creates the rather significant change to the seismic images of the reservoir model. Incorporated in this transformation is the effect of overburden and the processing sequences used in the study. The effect of processing is the most important factor. This is demonstrated by the significant differences between the two processed versions of the seismic data.

A good measure for the value of the interpretation results is the robustness of primary reflections. We see from the analysis that strong amplitude reflections, to a large degree, survive the effects of overburden and processing, whereas internal patterns and terminations are significantly changed. This is also the case for continuous primary reflections like reflections 1, 2, and 3. Based on this, continuity and amplitude should be the main criteria when picking key reflections. Terminations and patterns are not as reliable at this scale.

However, we also see that artificial continuity is easily created both by low-frequency effects (burial) and by processing. When the correct velocity model is used in reprocessing (Figures 9, 10), the section is cleaned up and appears much more realistic than the original version (Figure 8), but much false continuity is added to the section. This contributes to the creation of false low-angle terminations. Processing for improved lateral continuity should therefore be minimized because the seismic method itself will exaggerate continuity anyway.

External forms of the interpreted units are much more robust than internal patterns and terminations. In a situation where external forms are vague or lacking, the interpretation value of the internal patterns will be considerably reduced. In such a setting, it will be very difficult to distinguish primaries from noise.

Based on the results from this and other modeling studies (e.g., Biddle et al., 1992; Johansen et al., 1994, 2007), it is recommended to always establish a project specific interpretation library with a local translation from seismic data to geology. Forward modeling is here an excellent tool for testing the interpreted reservoir models. This also makes possible test processing on simulated seismic data in parallel with reprocessing of the real data. With such a procedure, the chance for model-based interpretation results will be significantly reduced.

Because of the size of the outcrops, the results from this analysis are relevant for reservoir-scale seismic interpretation and interpretation for prospect evaluation in mature basins. For seismic interpretation at a more regional scale, it is probably less relevant.

CONCLUSIONS

We found that the simulated seismic section, to a large degree, consists of seismic events not related to the reservoir model itself and that noise is the most important factor in forming the seismic facies. All reflections that cannot be ascribed directly to the reservoir model are here defined as noise. Overburden and processing effects dominated, and the low-frequency content complicated the seismic facies analyses. The main reason for this is that the analysis relies heavily on internal patterns and low-angle terminations. These are easily created by the seismic method itself, by effects originating in the overburden, and by noise and artifacts generated when processing the data.

Only the most robust seismic observations still exist after processing and burial to typical reservoir depth. Reliable observations are external form, strong amplitudes, and continuous reflections. However, continuity can be a pitfall for the interpreter because continuity is easily created also by reduced frequency content and processing. Internal pattern and terminations are commonly deceptive, and identification of boundaries based on predefined patterns of terminations does not work in this instance.

Uncritical use of seismic facies analysis in this case will create wrong reservoir models. Even with well control, it would be a great challenge to establish a correct reservoir model. Because of the scale of the outcrops in Van Keulenfjorden, these results are more relevant for seismic interpretation at reservoir scale than for interpretation for basin-scale exploration.

REFERENCES CITED

Biddle, K. T., W. Schlager, K. W. Rudolph, and T. L. Bush, 1992, Seismic model of a progradational carbonate platform, Pico di Vallandro, The Dolomites, northern Italy: AAPG Bulletin, v. 50, p. 14–30.

Cerjan, C., D. Kosloff, R. Kosloff, and M. Reshef, 1985, A nonreflecting boundary condition for discrete acoustic and elastic wave equations: Geophysics, v. 50, p. 705–708, doi:10.1190/1.1441945.

Dueholm, K. S., 1990, Multimodel stereo restitution: Photogrammetric Engineering and Remote Sensing, v. 56, p. 239–242.

Dueholm, K. S., 1992, Geologic photogrammetry using

standard small-frame cameras: Grønlands Geologiske Undersøkelse, v. 156, p. 7–17.
Dueholm, K. S., and T. Olsen, 1993, Reservoir analog studies using multimodel photogrammetry: A new tool for the petroleum industry: AAPG Bulletin, v. 77, p. 2023–2031.
Holberg, O., 1987, Computational aspects of the choice of operator and sampling interval for numerical differentiation in large-scale simulation of wave phenomena: Geophysical Prospecting, v. 35, p. 629–655.
Johansen, S. E., B. K. Ostisty, Ø. Birkeland, Y. F. Fedorovsky, V. N. Martirosjan, O. Bruun Christensen, S. I. Cheredeev, E. A. Ignatenko, and L. S. Margulis, 1993, Hydrocarbon potential in the Barents Sea region: Play distribution and potential, *in* T. O. Vorren, E. Bergsager, Ø. A. Dahl-Stamnes, E. Holler, B. Johansen, E. Lie, and T. B. Lund, eds., Arctic geology and petroleum potential: Norwegian Petroleum Society Special Publication 2, p. 273–320.
Johansen, S. E., S. Kibsgaard, A. Andresen, T. Henningsen, and J. R. Granli, 1994, Seismic modeling of a strongly emergent thrust front: West Spitsbergen fold belt, Svalbard: AAPG Bulletin, v. 78, p. 1018–1027.
Johansen, S. E., E. Granberg, D. Mellere, B. Arntsen, and T. Olsen, 2007, Decoupling of seismic reflectors and stratigraphic timelines: A modeling study of Tertiary strata from Svalbard: Geophysics, v. 72, no. 5, p. 273–280.
Kellog, H. E., 1975, Tertiary stratigraphy and tectonism in Svalbard and continental drift: AAPG Bulletin, v. 59, p. 465–485.
Mellere, D., A. Breda, and R. Steel, 2003, Fluvially incised shelf-edge deltas and linkage to upper-slope channels (central Tertiary basin in Spitsbergen), *in* H. Roberts et al., eds., Global significance and future exploration potential: Gulf Coast Section-SEPM Special Publication, v. 23, p. 231–266.
Mitchum, R. M., P. R. Vail, and S. Thompson, 1977, Seismic stratigraphy and global changes of sea level: Part 2. The depositional sequence as a basic for stratigraphic analysis, *in* C. E. Payton, ed., Seismic stratigraphy: Application to hydrocarbon exploration: AAPG Memoir 26, p. 53–62.
Mittet, R., and R. Renlie, 1996, High-order finite-difference modeling of multipole logging in formations with anisotropic attenuation and elasticity: Geophysics, v. 61, p. 21–33, doi:10.1190/1.1443942.
Myhre, A. M., O. Eldholm, and E. Sundvor, 1982, The margin between Senja and Spitsbergen fracture zones: Implications from plate tectonics: Tectonophysics, v. 89, p. 33–50, doi:10.1016/0040-1951(82)90033-6.
Sheriff, R. E., 1977, Limitations on resolution of seismic reflections and geologic detail derivable from them, *in* C. E. Payton, ed., Seismic stratigraphy: Application to hydrocarbon exploration: AAPG Memoir 26, p. 3–14.
Spencer, A. M., P. C. Home, and L. T. Berglund, 1984, Tertiary structural development of the western Barents Shelf, Troms to Svalbard, *in* A. M. Spencer, ed., Petroleum geology of the North European margin: London, Norwegian Petroleum Society, p. 199–209.
Steel, R. J., and T. Olsen, 2002, Clinoforms, clinoform trajectories and deep-water sands, *in* J. M. Armentrout and N. C. Rosen, eds., Sequence-stratigraphic models for exploration and production: Evolving methodology, emerging models and application histories: Gulf Coast Section-SEPM Special Publication, v. 22, p. 367–381.
Steel, R., J. Gjelberg, W. Helland-Hansen, K. Kleinspehn, A. Nøttvedt, and M. R. Larsen, 1985, The Tertiary strike-slip basins and orogenic belt of Spitsbergen, *in* K. T. Biddle and N. Christie-Buck, eds., Strike-slip deformation, basins formation and sedimentation: SEPM Special Publication 37, p. 339–358.
Steel, R., D. Mellere, P. Plink, J. Crabaugh, J. Deibert, and M. Schellpeper, 2000, Deltas vs. rivers on at shelf edge: Their relative contributions to the growth of shelf margins and basin-floor fans (Barremian and Eocene, Spitzbergen): Gulf Coast Association-SEPM Special Publication 28, p. 981–1009.
Vail, P. R., and R. M. Mitchum Jr., 1977, Seismic stratigraphy and global changes of sea level: Part 1. Overview, *in* C. E. Payton, ed., Seismic stratigraphy: Application to hydrocarbon exploration: AAPG Memoir 26, p. 51–52.
Vail, P. R., R. M. Mitchum Jr., R. G. Todd, J. M. Widmier, S. Thomson III, L. B. Sangree, J. N. Bubb, and W. G. Hatlelid, 1977, Seismic stratigraphy and global changes of sea level, *in* C. E. Payton, ed., Seismic stratigraphy: Applications to hydrocarbon exploration: AAPG Bulletin Memoir 26, p. 51–212.
Vien, P. T., E. Tjåland, B. Arntsen, and S. Johansen, 1997, Optimum seismic processing of modeled outcrop data from van Keulenfjord, Svalbard: 67th Annual Meeting of the Society of Exploration Geophysicists, Dallas, Texas, p.1395–1398.